27th International Congress
on Sound and Vibration
The annual congress of
the International Institute
of Acoustics and Vibration (IIAV)

11-16 July, 2021

ICSV27

Annual Congress of the International Institute of Acoustics and Vibration (IIAV)

A COUPLED 3D FINITE ELEMENT MODEL OF THE SOUND PRODUCTION BY MALLET PERCUSSION INSTRUMENTS

Péter Rucz, Mihály Ádám Ulveczki

Budapest University of Technology and Economics, Dept. of Networked Systems and Services, H-1117 Budapest, Hungary, e-mail: rucz@hit.bme.hu

The sound production in mallet percussion instruments involves mechanical vibrations, acoustical resonance, and radiation inherently coupled. The source of energy is the mallet that excites mechanical oscillations in the sound bar when the player hits one of the notes. The sound bar in itself is an inefficient radiator, therefore acoustical resonators are applied in order to reinforce the radiated sound. There are various challenges in modeling tuned idiophone instruments, including the nonlinear interaction of the mallet and the sound bar, the orthotropic behavior of the material of the bars, and the sound radiation into the half-open acoustical space. In this contribution the coupled finite element model of a xylophone is examined in detail. The three-dimensional model consists of mechanical and acoustical finite elements, and infinite acoustical elements that emulate free field radiation conditions. The coupled system is solved in the time domain with exploiting the benefits of the modal basis for reducing the size of the system of equations. The paper demonstrates the capabilities of the model, emphasizing the effect of two-way vibroacoustic coupling between the sound bar and the resonator. By analyzing the energy balance of the mechanical and acoustical subsystems the effect of tuning the resonator is investigated. The three-dimensional sound bar model is further exploited by studying the effect of the excitation of the torsional modes of the bar. Finally, synthesized sound samples illustrate the applicability of the model for physics-based sound synthesis.
Keywords: finite elements, mallet percussion instruments, vibroacoustic coupling

1. Introduction

Mallet percussion instruments belong to the family of tuned idiophones and they produce sound by the radiation of their struck sound bars. The vertical bending modes of the sound bars are tuned by a characteristic undercut to attain a harmonic ratio of $1:4:10$ or $1:3:9$ of the frequencies of the first three partials. The vertical modes of vibration are responsible for radiating most of the acoustical energy and the sound can also be reinforced by tubular or cavity resonators.

Numerical simulations of xylophone bars based on a one-dimensional finite difference method were introduced in [1], where the nonlinear interaction of the mallet and the sound bar was also examined in detail both by experiments and simulations. Then, in [2] the model was extended by a tubular resonator that was also described as a 1D system. The latter contribution assumed that the back-coupling effect of the resonator on the bar is negligible, which is a specific property of xylophone bars in the higher frequency range, and cannot be generalized to all mallet percussion instruments.

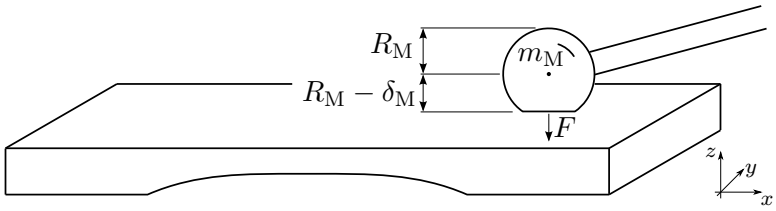

Figure 1: Deformation of the mallet head during the mallet–sound bar interaction

This paper presents a 3D coupled finite element model of the sound production by mallet percussions. The proposed model takes both forward and backward coupling (to and from the resonator) into account. The 3D representation of the sound bar allows for observing the torsional modes of the bar as well. The capabilities of the model are demonstrated in the sequel by examining an Orff xylophone.

2. Physical model

2.1 Mechanical system

A three-dimensional mechanical model, based on the Navier – Cauchy equations for linear elasticity is considered. The equation of motion in the solid is expressed as

$$\nabla \cdot \boldsymbol{\sigma} + \boldsymbol{b} = \rho \ddot{\boldsymbol{u}}, \tag{1}$$

where $\boldsymbol{\sigma}$ is the stress tensor, $\boldsymbol{b}$ are the body forces acting on the solid, ρ is density of the material, and $\boldsymbol{u}$ is the displacement. The stress–strain relationship is given by the generalized Hooke law as

$$\boldsymbol{\sigma} = \mathsf{C} : \boldsymbol{\varepsilon}, \tag{2}$$

where C is the stiffness tensor of the material, and $\boldsymbol{\varepsilon} = \frac{1}{2}[\nabla \boldsymbol{u} + (\nabla \boldsymbol{u})^{\mathrm{T}}]$ is the strain tensor. Viscoelastic losses are incorporated by replacing $\boldsymbol{\varepsilon}$ with $\boldsymbol{\varepsilon} + \eta \dot{\boldsymbol{\varepsilon}}$ in (2), with η denoting the viscosity.

2.2 Acoustical model

The propagation of acoustical waves is described by the wave equation

$$\nabla^2 p - \frac{1}{c^2} \ddot{p} = 0, \tag{3}$$

where p is the sound pressure and c is the speed of sound. At the interfaces with the resonator and the sound bar, the boundary conditions are defined using the Euler equation

$$\nabla p + \rho_0 \dot{\boldsymbol{v}} = \boldsymbol{0}, \tag{4}$$

where ρ_0 is the equilibrium density of air, and $\boldsymbol{v}$ is the particle velocity, whose normal component must be equal to that of the mechanical structure. The walls of the resonator are assumed to be non-moving.

2.3 Mallet–sound bar interaction

The geometry of the mallet–sound bar interaction is sketched in Figure 1. The mallet head is assumed to hit the sound bar having a prescribed initial velocity $v_\mathrm{M}(0)$. Following [1], the compression of the mallet head δ_M during the interaction with the sound bar is expressed from the interaction force F using Hertz's law of contact written for two colliding spheres as

$$\delta_\mathrm{M} = \left[F^2 D^2 \left(\frac{1}{R_\mathrm{B}} + \frac{1}{R_\mathrm{M}} \right) \right]^{1/3}, \tag{5}$$

where the constant D is calculated from the elastic material properties of the mallet head and the bar, and R_B and R_M denote the radius of the sound bar and that of the mallet head, respectively. The equivalent radius of the sound bar considered as a sphere can be taken as infinite and hence the interaction force is expressed from the compression of the mallet head as

$$F = \frac{\sqrt{R_\mathrm{M}}}{D}\delta_\mathrm{M}^{3/2} = K_\mathrm{M}\delta_\mathrm{M}^{3/2}, \tag{6}$$

where K_M was introduced to denote the equivalent stiffness of the mallet head.

The equation of motion is written for the mallet head as

$$m_\mathrm{M}\ddot{u}_\mathrm{M} = F_\mathrm{M} = \begin{cases} -K_\mathrm{M}\left|u_\mathrm{B} - u_\mathrm{M}\right|^{3/2} & \text{if} \quad u_\mathrm{M} < u_\mathrm{B}, \\ 0 & \text{otherwise.} \end{cases} \tag{7}$$

The displacement of the mallet head and that of the bar at the point of the interaction are denoted by u_M and u_B, respectively, while F_M denotes the force acting on the mallet head.

As seen, the interaction force depends non-linearly on the compression of the mallet head. Hence, the strength of the hit (i.e., the initial velocity of the mallet head) affects both the level and the timbre of the radiated sound. From the viewpoint of numerical modeling, the nonlinearity introduces a challenge.

3. Finite element formulation

3.1 The coupled system

The governing equations of the mechanical system are discretized by a standard Galerkin finite element method (FEM). A similar approach is used in case of the acoustical system; however, as the sound bar radiates into open space, the acoustical domain is unbounded, which necessitates applying special boundary conditions at the open boundaries of the truncated domain disctretized by finite elements. Here, the infinite element method (IEM) is utilized based on the formulation given in [3].

To arrive at a fully coupled system, two-way interactions between the sound bar and the surrounding sound field need to be taken into account. First, the acoustical pressure exerts force on the surface of the sound bar in its normal direction. Second, the motion of the bar appears as a velocity boundary condition for the acoustical system. Only the motion in the normal direction generates acoustical waves, and the normal particle velocity is taken to be equal to the normal vibration velocity of the sound bar. The discretization leads to a coupled system of linear equations written in matrix form as

$$\begin{aligned} \mathbf{K}_\mathrm{m}\mathbf{u} + \mathbf{C}_\mathrm{m}\dot{\mathbf{u}} + \mathbf{M}_\mathrm{m}\ddot{\mathbf{u}} &= \mathbf{F}_\mathrm{m}\left(\mathbf{f} + \mathbf{A}_\mathrm{m}\mathbf{p}\right) \\ \mathbf{K}_\mathrm{a}\mathbf{p} + \mathbf{C}_\mathrm{a}\dot{\mathbf{p}} + \mathbf{M}_\mathrm{a}\ddot{\mathbf{p}} &= -\mathbf{F}_\mathrm{a}\mathbf{A}_\mathrm{a}\ddot{\mathbf{u}}, \end{aligned} \tag{8}$$

where $\mathbf{K}$, $\mathbf{C}$, and $\mathbf{M}$ are the stiffness, damping, and mass matrices, respectively, and the subscripts m and a refer to the mechanical and acoustical subsystems. The damping matrix $\mathbf{C}_\mathrm{a}$ appears due to the application of the IEM. The vectors $\mathbf{u}$ and $\mathbf{p}$ denote the coefficients of the displacement and the acoustical pressure, while $\mathbf{f}$ contains the weights of the force distribution exerted by the mallet over the surface of the sound bar. The matrices $\mathbf{F}$ contain surface integrals of the shape functions. Conservative interpolation between the mechanical and acoustical meshes is performed by multiplications with the matrices $\mathbf{A}$.

3.2 Modal description and solution

Both the displacement weights of the sound bar $\mathbf{u}$ and the sound pressure weights $\mathbf{p}$ are written in a truncated modal basis using the mode shapes ψ and modal coordinates q as

$$\mathbf{u} \approx \sum_{i=1}^{n_\mathrm{m}} \psi_{\mathrm{m},i} q_{\mathrm{m},i} = \mathbf{\Psi}_\mathrm{m}\mathbf{q}_\mathrm{m} \qquad \text{and} \qquad \mathbf{p} \approx \sum_{i=1}^{n_\mathrm{a}} \psi_{\mathrm{a},i} q_{\mathrm{a},i} = \mathbf{\Psi}_\mathrm{a}\mathbf{q}_\mathrm{a}, \tag{9}$$

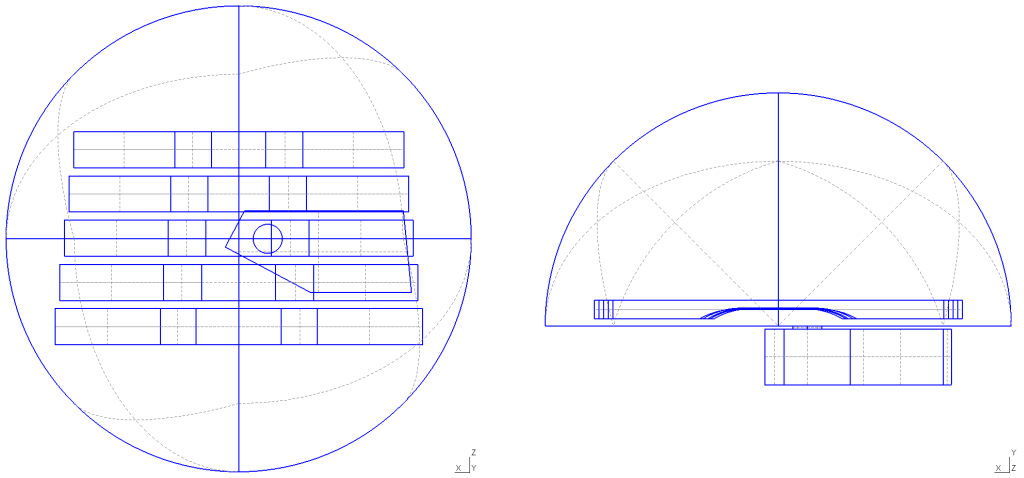

Figure 2: Sketch of the geometry of the coupled finite element model. Left: top view. Right: side view. The middle sound bar is hit by the mallet, the other sound bars are considered as perfectly rigid.

where the number of modes are n_m and n_a in case of the mechanical and acoustical systems, respectively. The matrices $\mathbf{\Psi}_\mathrm{m}$ and $\mathbf{\Psi}_\mathrm{a}$ contain the mechanical and acoustical eigenmodes in their columns.

The coupled system of equations (8) is converted into the modal basis by applying the modal representation (9) and multiplying the mechanical equation by $\mathbf{\Psi}_\mathrm{m}^\mathrm{H}$ and the acoustical equation by $\mathbf{\Psi}_\mathrm{a}^\mathrm{H}$ from the left. The coupled equation is rearranged and written in the modal system as

$$\begin{aligned}\begin{bmatrix} \mathbf{\Psi}_\mathrm{m}^\mathrm{H}\mathbf{K}_\mathrm{m}\mathbf{\Psi}_\mathrm{m} & -\mathbf{\Psi}_\mathrm{m}^\mathrm{H}\mathbf{F}_\mathrm{m}\mathbf{A}_\mathrm{m}\mathbf{\Psi}_\mathrm{a} \\ \mathbf{0} & \mathbf{\Psi}_\mathrm{a}^\mathrm{H}\mathbf{K}_\mathrm{a}\mathbf{\Psi}_\mathrm{a} \end{bmatrix} \begin{Bmatrix} \mathbf{q}_\mathrm{m} \\ \mathbf{q}_\mathrm{a} \end{Bmatrix} + \begin{bmatrix} \mathbf{\Psi}_\mathrm{m}^\mathrm{H}\mathbf{C}_\mathrm{m}\mathbf{\Psi}_\mathrm{m} & \mathbf{0} \\ \mathbf{0} & \mathbf{\Psi}_\mathrm{a}^\mathrm{H}\mathbf{C}_\mathrm{a}\mathbf{\Psi}_\mathrm{a} \end{bmatrix} \begin{Bmatrix} \dot{\mathbf{q}}_\mathrm{m} \\ \dot{\mathbf{q}}_\mathrm{a} \end{Bmatrix} \\ + \begin{bmatrix} \mathbf{\Psi}_\mathrm{m}^\mathrm{H}\mathbf{M}_\mathrm{m}\mathbf{\Psi}_\mathrm{m} & \mathbf{0} \\ \mathbf{\Psi}_\mathrm{a}^\mathrm{H}\mathbf{F}_\mathrm{a}\mathbf{A}_\mathrm{a}\mathbf{\Psi}_\mathrm{m} & \mathbf{\Psi}_\mathrm{a}^\mathrm{H}\mathbf{M}_\mathrm{a}\mathbf{\Psi}_\mathrm{a} \end{bmatrix} \begin{Bmatrix} \ddot{\mathbf{q}}_\mathrm{m} \\ \ddot{\mathbf{q}}_\mathrm{a} \end{Bmatrix} = \begin{Bmatrix} \mathbf{\Psi}_\mathrm{m}^\mathrm{H}\mathbf{F}_\mathrm{m}\mathbf{f} \\ \mathbf{0} \end{Bmatrix}. \end{aligned} \tag{10}$$

With denoting the combined vector of modal coordinates by $\mathbf{q}$ and the right hand side vector by $\mathbf{g}$, equation (10) is written as

$$\mathbf{K}\mathbf{q} + \mathbf{C}\dot{\mathbf{q}} + \mathbf{M}\ddot{\mathbf{q}} = \mathbf{g}. \tag{11}$$

Equations (7) and (11) are solved by the semi-implicit Newmark time stepping scheme [4]. Initially, the sound bar is motionless and the sound pressure is zero everywhere, while the mallet descends towards the sound bar with a prescribed velocity $v_\mathrm{M}(0)$. To model the nonlinear interaction of mallet and sound bar accurately, the time step size is chosen to be significantly smaller during the contact than that during free vibration. A few tens of modes were found to be sufficient for representing both subsystems in the musically relevant range of frequencies. Thus, the modal basis efficiently reduces the number of unknowns and allows for performing a large number of time steps at moderate computational cost.

4. Results

In the sequel the results of simulations using the geometry of an Orff xylophone model shown in Figure 2 are evaluated. The model contains only the $\mathrm{F4}$ ($\approx 349\,\mathrm{Hz}$) note of the 13 sound bars and resonators that are tuned to the diatonic scale in the range $\mathrm{C4}-\mathrm{A5}$. The geometry consists of 1) a Helmholtz cavity resonator with a circular opening, a very short neck, and an irregularly shaped base, 2) a hemisphere volume representing the exterior sound field and 3) five sound bars. It was found previously [5] that the presence of neighboring sound bars can have a significant effect on the eigenfrequency of the resonator, thus, beside the excited middle sound bar, the neighboring bars are also included in the model.

Component	Parameter	Symbol	Value
Mallet	Mass	m_M	$25 \times 10^{-3}\,\mathrm{kg}$
	Stiffness	K_M	$5 \times 10^7\,\mathrm{N/m^{3/2}}$
	Initial velocity	$v_\mathrm{M}(0)$	$1\,\mathrm{m/s}$
	Interaction area	S_eff	$3.88\,\mathrm{mm^2}$
	Interaction time	T_int	$0.6\,\mathrm{ms}$

Component	Parameter	Symbol	Value
Sound bar	Mass	m_B	$96.7 \times 10^{-3}\,\mathrm{kg}$
	Fundamental	$f_{\mathrm{m},1}$	$348.8\,\mathrm{Hz}$
	Damping	$\xi_\mathrm{m}, 1$	2.57×10^{-4}
Resonator	Fundamental	$f_{\mathrm{a},1}$	$349.1\,\mathrm{Hz}$
	Damping	$\xi_{\mathrm{a},1}$	8.8×10^{-3}

Table 1: Representative parameters of the simulated coupled vibroacoustic model

The mesh of the sound bar is structured and consists of linear hexahedra elements. An orthotropic material model is utilized for modeling the rosewood bar with the elastic moduli tuned to match the measured eigenfrequencies of the bar. The unstructured acoustical mesh is generated by the parametric mesh generation tool Gmsh [6] and consists of linear tetrahedra. Infinite elements are attached to the outer surface of the hemisphere shown in Figure 2 to emulate free field radiation conditions.

Table 1 summarizes the representative parameters of the simulated system. Some of the listed parameters are varied in the examinations discussed in the following. The sampling frequency of the time stepping algorithm is chosen as $f_\mathrm{s} = 48\,\mathrm{kHz}$ (time step $\Delta t = 20.83\,\mu\mathrm{s}$) during free vibration, and an oversampling of 100–200 times is applied during the short period of mallet–sound bar interaction.

4.1 Analysis of the energy balance

In order to validate the proposed solution strategy and its implementation, the energy balance of the coupled system is investigated first. By conservation of energy, the balance is written in the form

$$\Sigma E = \underbrace{E_{\mathrm{M},p}(t) + E_{\mathrm{M},k}(t)}_{\text{Mallet}} + \underbrace{E_{\mathrm{B},p}(t) + E_{\mathrm{B},k}(t) + W_\mathrm{B}(t)}_{\text{Bar with losses}} + \underbrace{E_{\mathrm{A},p}(t) + E_{\mathrm{A},k}(t) + W_\mathrm{A}(t)}_{\text{Sound field and radiation}} = \text{constant}. \tag{12}$$

Subscripts p and k refer to potential and kinetic energies, respectively. The energy dissipated by internal losses of the sound bar is denoted by W_B, and the radiated acoustical energy is W_A. The mechanical energy of the mallet head is calculated from the compression δ_M and the velocity v_M, whereas the energy stored in the mechanical and acoustical systems is computed making use of the finite element system matrices and the simulated displacement and pressure fields. The radiated acoustical power is found by integrating the intensity over the hemisphere surface shown in Figure 2.

The left diagram of Figure 3 depicts the energy relations during the mallet–sound bar interaction. At $t = 0$ there is no energy stored in the sound bar, and the mallet head has only kinetic energy. As the mallet head reaches the bar, it transfers its kinetic energy to mechanical energy stored in the sound bar, and, at the same time, as the head of the mallet is deformed, the mallet head also stores potential energy. Due to energy transfer to the sound bar and the motion of the bar, the time instance when the kinetic energy of the mallet is minimal differs from the time instance when its potential energy is maximal. When the mallet leaves the sound bar, some of its potential energy is restored as kinetic energy.

The energy relations during free vibration and sound radiation are shown in the right hand side of Figure 3. The energy transferred from the mallet head to the sound bar during the interaction, is converted into potential and kinetic energy of the sound field in the initial phase of sound radiation, while energy is dissipated by the mechanical losses of the sound bar and the sound radiation. It is worth observing in this case that the initial kinetic energy of the mallet is converted quite efficiently into radiated acoustical energy thanks to the well tuned resonator. The radiated acoustical energy is more than three times greater than the energy dissipated by mechanical losses of the sound bar. It is shown in the next section that this relation changes significantly with the tuning of the resonator.

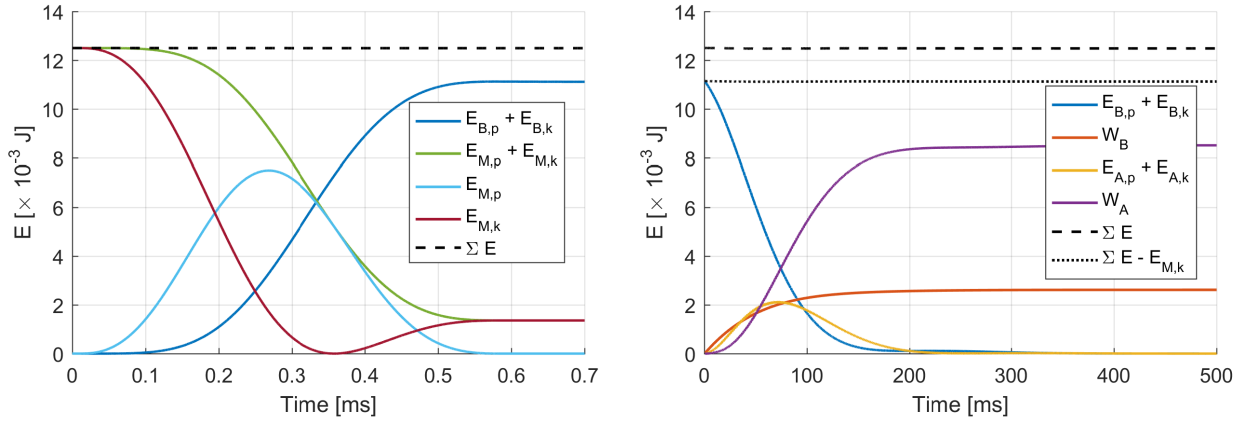

Figure 3: Energy relations of the coupled mallet–sound bar–resonator finite element system consisting of a wooden sound bar and a tuned cavity resonator. Left: during mallet–sound bar interaction. Right: free vibration.

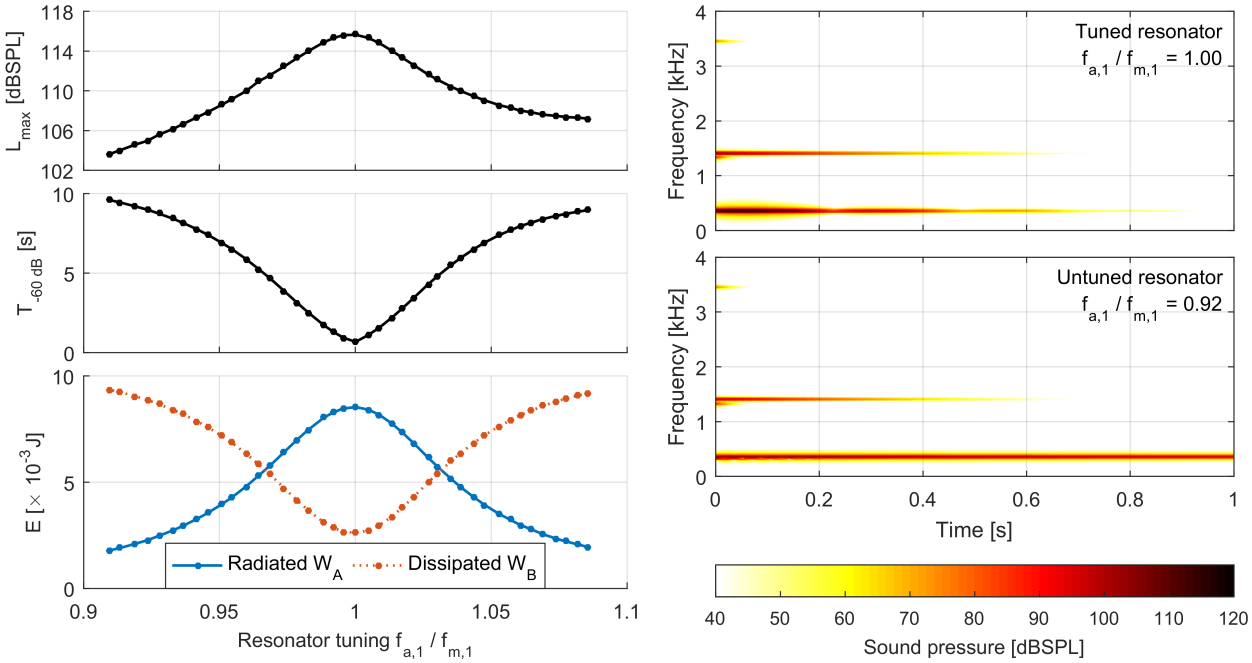

Figure 4: Effect of tuning the resonator on the peak level of the radiated sound (top left), decay time (center left), radiated and dissipated energy (bottom left) and the spectrogram of the radiated sound (right).

This simulation demonstrates well that energy is conserved in the implemented coupled model and time stepping scheme. Due to the nonlinear interaction of the mallet head and the sound bar, very high sampling frequency is necessary for the short duration of the contact.

4.2 Effect of tuning the resonator

The effect of changing the tuning of the resonator on the radiated sound is examined by varying the depth of the Helmholtz resonator. The tuning is varied in the range $0.9 < f_{\mathrm{a},1}/f_{\mathrm{m},1} < 1.1$, which corresponds to ± 1.5 semitones. In comparison, it was found experimentally that removing the sound bars increases the natural resonance frequency of the resonator by one semitone.

Figure 4 shows the effect of changing the tuning of the resonator. The peak sound pressure level $L_{\max}$, evaluated at single point at $0.25\,\mathrm{m}$ distance above the center of the sound bar, weighted by exponential averaging with a characteristic time of $T_{\mathrm{rms}} = 15\,\mathrm{ms}$, illustrates that a tuned resonator can amplify

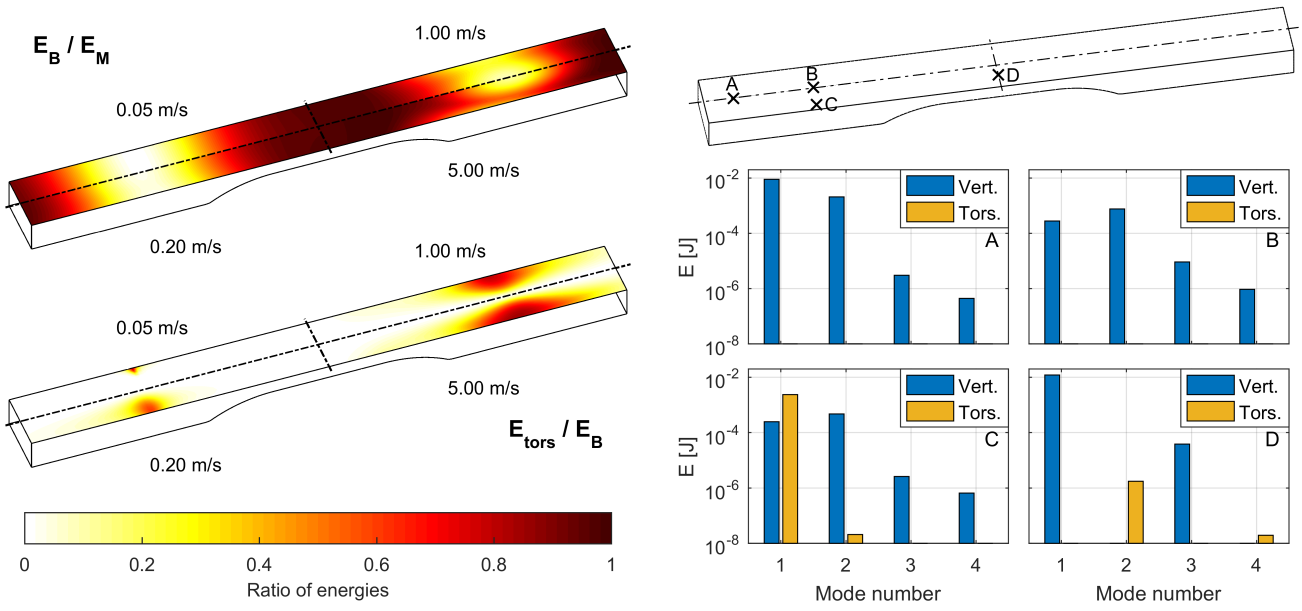

Figure 5: Excitation of torsional modes of the sound bar by varying the position and strength of the mallet. Top left: ratio of the total mechanical energy of the bar E_B and that of the mallet. Bottom left: Share of torsional modes from the mechanical energy of the bar. Right: the mechanical energy of different modes with $v_\mathrm{M}(0) = 1\,\mathrm{m/s}$.

the sound by as much as $15\,\mathrm{dB}$. It is also visible that the tuning of the resonator is a key factor of the decay time of the sound, displayed as $T_{-60\,\mathrm{dB}}$ and referring to the time duration in which the sound pressure level decays $60\,\mathrm{dB}$. While in the case of an untuned resonator the decay time is close to $10\,\mathrm{s}$, for a well tuned resonator it reduces to $0.7\,\mathrm{s}$. The effect on the peak level and decay time was also investigated experimentally by Bork [7]. The simulation results presented in Figure 4 show an excellent qualitative and quantitative agreement with the measured data.

By examining the energy relations of the system, it is found that with tuning the resonator the radiated acoustical energy is also significantly increased, while the energy dissipated by the mechanical losses of the sound bar is remarkably reduced. When the sound bar transfers energy efficiently to the sound field, radiation happens more rapidly than dissipation inside the bar. The spectrogram plots show that it is the fundamental component that is most affected by the resonator due to its tuning and the viscoelastic losses being significantly greater in case of higher partials.

4.3 Excitation of torsional modes

Beside the vertical modes being responsible for sound radiation, the 3D model of the sound bar allows for examining the role of torsional modes too. While these modes do not radiate sound efficiently, their excitation may result in a sound of poor quality as they can take away a significant amount of energy.

The left hand side of Figure 5 shows the efficiency of the excitation of different modes with varying the position of the hit by the mallet. Each colored point on the surface represents a distinct position of the mallet hit. Four cases with different initial velocities are plotted over the four quadrants. The energy relations right after the interaction with the mallet are shown. With increasing the initial velocity of the mallet head, the interaction time is reduced and modes having higher frequencies become also efficiently excited. It is seen in the top left diagram that the mallet head can transfer its kinetic energy quite efficiently to the sound bar, except near the nodal lines of the first vertical mode of the bar. Near the latter locations, torsional modes can quite efficiently be excited, especially by stronger hits by the mallet.

The right hand side of Figure 5 displays the distribution of mechanical energy among the first four vertical and torsional modes when hitting the sound bar at different position with $v_\mathrm{M}(0) = 1\,\mathrm{m/s}$.

Positions A and B are on the longitudinal axis of the bar and torsional modes are not excited at all by hitting the bar at these locations. Points B and C are near the nodal line of the first vertical mode and hence the second vertical mode is stronger than the first. In case of position C the first torsional mode becomes the strongest. Finally, point D is at half the length of the bar where the even vertical modes have nodal lines, thus, the first and third vertical modes have the most energy.

5. Conclusions

A three-dimensional coupled finite element model for the simulation of sound production by mallet percussion instruments was discussed in this paper. The proposed model takes the two-way coupling of the sound bar and the resonator into account, uses the truncated modal basis of both subsystems, and solves the equations of motion including the nonlinear interaction with the mallet in the time domain.

An Orff xylophone model was investigated in different configurations. By analyzing the energy balance of the system it was shown that energy is conserved by the simulation both during contact and free vibration. The effect of tuning the resonator was examined and the computations gave an excellent agreement with experimental data, highlighting the importance of the two-way coupling. By varying the position and the strength of the hit by the mallet it was found that torsional modes are efficiently excited near the nodal line of the first vertical mode, especially in case of strong hits.

Acknowledgments

P. Rucz gratefully acknowledges the support of the Bolyai János research grant provided by the Hungarian Academy of Sciences. Supported by the ÚNKP–19–4 new national excellence program of the Ministry for Innovation and Technology.

REFERENCES

1 A. Chaigne and V. Doutaut. Numerical simulations of xylophones. I. Time-domain modeling of the vibrating bars. *Journal of the Acoustical Society of America*, 101(1):539–557, 1997.

2 V. Doutaut, D. Matignon, and A. Chaigne. Numerical simulations of xylophones. II. Time-domain modeling of the resonator and of the radiated sound pressure. *Journal of the Acoustical Society of America*, 104(3):1633–1647, 1998.

3 R. J. Astley, G. J. Macaulay, J-P. Coyette, and L. Cremers. Three-dimensional wave-envelope elements of variable order for acoustic radiation and scattering: Part I. Formulation in the frequency domain. *Journal of the Acoustical Society of America*, 103:49–63, 1998.

4 N. M. Newmark. A method of computation for structural dynamics. *ASCE Journal of the Engineering Mechanics Division*, 85:67–94, 1959.

5 P. Rucz, J. Angster, and A. Miklós. Finite element simulation of radiation impedances with applications for musical instrument design. In M. Kob, editor, *ISMA2019 International Symposium on Music Acoustics*, pages 275–282, Detmold, Germany, 2019. Deutsche Gesellschaft für Akustik e.V. (DEGA).

6 C. Geuzaine and J.-F. Remacle. Gmsh: a three-dimensional finite element mesh generator with built-in pre- and post-processing facilities. *International Journal for Numerical Methods in Engineering*, 79(11):1309–1331, 2009.

7 I. Bork. Practical tuning of xylophone bars and resonators. *Applied Acoustics*, 46:103–127, 1995.